CONSTRAINED BURN OPTIMIZATION FOR THE INTERNATIONAL SPACE STATION

Aaron J. Brown[*] **and Brandon A. Jones**[†]

In long-term trajectory planning for the International Space Station (ISS), translational burns are currently targeted sequentially to meet the immediate trajectory constraints, rather than simultaneously to meet all constraints, do not employ gradient-based search techniques, and are not optimized for a minimum total delta-v (Δv) solution. An analytic formulation of the constraint gradients is developed and used in an optimization solver to overcome these obstacles. Two trajectory examples are explored, highlighting the advantage of the proposed method over the current approach, as well as the potential Δv and propellant savings in the event of propellant shortages.

INTRODUCTION

The first module of the ISS, *Zarya* ("sunrise" in Russian), was launched on November 20, 1998 from Baikonur Cosmodrome in Kazakhstan. It was launched into a 400 km altitude, roughly circular orbit, and an inclination of $51.6°$. Each module that followed was launched into the same orbit and added to the ISS main body. With only minor fluctuations in altitude (between roughly 330 km and 420 km), the ISS has ostensibly remained in the same orbit ever since.

The primary perturbing forces acting on the ISS orbit include Earth's non-spherical gravity, third-body perturbations from the Sun and Moon, and atmospheric drag. Except for the secular effect of J_2 and atmospheric drag, the effects of these forces on the ISS orbit are either relatively small in magnitude, periodic in nature, or both, and therefore do not affect the orbit's long-term evolution.

The ISS orbit is planned and maintained in part by the ISS Trajectory Operations (TOPO) group at the NASA Johnson Space Center. TOPO personnel routinely generate look-ahead trajectory plans for the ISS, ranging in length from six weeks to almost two years. Each plan contains the trajectory-related events that occur during the plan's time frame, including visiting vehicle launches, dockings, undockings, landings, and ISS translation burns.

One of the goals in generating a given plan is to target the ISS translation burns that satisfy the ISS trajectory constraints. The burns are scheduled to occur on agreed-to dates by the ISS International Partners (IPs). The constraints are imposed by Russian Soyuz (crewed) and Progress (cargo) vehicle launches and Soyuz vehicle landings, which require the ISS orbit to fall within a specified Longitude of Ascending Node (LAN) range on the day of the launch or landing. The ISS LAN itself shifts

---

[*]Aerospace Engineer, Aeroscience and Flight Mechanics Division, NASA Johnson Space Center, Mail Code EG6, 2101 NASA Parkway, Houston, TX 77058.

[†]Assistant Professor, Department of Aerospace Engineering and Engineering Mechanics, The University of Texas at Austin, Austin, TX 78712

approximately $23.3°$ westward per orbit due to the combination of Earth rotating to the east and the ISS orbit precessing to the west. Additionally, one or more semi-major axis (SMA) altitude constraints may be imposed on the trajectory. These constraints ensure the ISS achieves a certain mean SMA altitude on a certain date, or maintains a mean SMA altitude across a range of dates.

Unfortunately, the legacy software used by TOPO personnel for targeting these burns does not utilize any gradient-based search techniques for finding feasible burn solutions. This makes for a cumbersome process in which burns are targeted manually rather than automatically, thereby forcing users to find burn solutions sequentially (i.e, burn by burn), rather than simultaneously for all burns. Furthermore, this process does not at all enable finding optimal solutions that minimize total Δv over the trajectory plan time frame.

In recent years, however, a large-scale project has been underway to replace this legacy software with a set of trajectory tools that can utilize differential correction to find feasible burn solutions, or can be embedded in a larger optimization framework to find optimal burn solutions. The goal of this work is to provide the mathematical formulation of the constraint gradients in the ISS burn optimization problem, and to use these gradients in an optimization solver to find either feasible or minimum Δv burn solutions for ISS trajectory planning.

Reboost Burn Modeling

In ISS trajectory planning, translation burns are modeled in the Local-Vertical, Local Horizontal (LVLH) reference frame. The LVLH frame is centered on the vehicle, with the Z-axis (the LV axis) opposite the radius vector (i.e. down), the Y-axis opposite the orbit's angular momentum vector, and the X-axis (i.e. the LH-axis) completing the right-handed system, as shown in Figure 1.
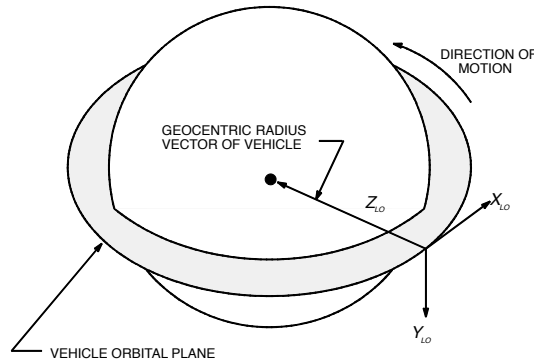

Figure 1: LVLH Coordinate System[1]

Each burn is modeled as impulsive, with $\Delta v \geq 0$, and in a fixed direction defined by LVLH yaw (ψ) and pitch (θ) angles in a yaw-pitch-roll sequence. These angles are typically small, resulting in a posigrade or reboost burn. Reboost burns serve to restore orbit altitude lost due to atmospheric drag. Each burn is scheduled to occur on a specific date, with the burn's Time of Ignition (TIG) on that date occurring at apogee ($\nu = 180°$) of Daily Orbit 1 (DO1). Since the ISS orbital period is roughly 92 minutes, there are either 15 or 16 DOs each day. On a given day, DO1 is defined to be the first orbit with a Longitude of Ascending Node (LAN) that is west of $20°E$. Burns are nominally scheduled to occur on DO1 to allow for their visibility via Russian ground stations.

2

Burn Optimization Problem Statement

Given the ISS reboost burn model in the previous section, the burn optimization problem can be stated as follows. Given a fixed timespan from t_0 to t_f, with n reboost burns to occur on fixed dates $t_1, t_2, \ldots, t_n$,

$$\text{minimize } J = \sum_{i=1}^{n} \Delta v_i. \tag{1}$$

Since each $\Delta v_i \geq 0$, J in Equation 1 is effectively the ℓ_1-norm of an n-element vector containing the Δv magnitudes.

The controls in this problem are the burn Δv magnitudes and the constraints, as noted in the Introduction, are given by the Russian Soyuz and Progress launches, and Soyuz vehicle landings.

- Soyuz launch LAN constraints: $13.9° \leq \lambda \leq 15.4°$

- Soyuz landing LAN constraints: $12.7° \leq \lambda \leq 16.5°$

- Progress launch LAN constraints: $26.5° \leq \lambda \leq 38.9°$

- SMA altitude constraints

Given the cost function J in Equation 1, the objective partial derivatives are easily given by

$$\frac{\partial J}{\partial (\Delta v_i)} = 1, \quad i = 1, \ldots, n. \tag{2}$$

The constraint partial derivatives are now developed by first examining the total state differential for a generic trajectory segment. This differential is used repeatedly to formulate state partial derivatives, which are then used to arrive at the desired constraint partial derivative expressions.

Total State Differential for a Generic Trajectory Segment

The development in this sub-section follows and expands on work done by Ocampo and Munoz.[2] Consider the generic trajectory segment in Figure 2. Let the state $\mathbf{x}$ be defined as

$$\mathbf{x} \triangleq \begin{bmatrix} \mathbf{r}^T & \mathbf{v}^T \end{bmatrix}^T, \tag{3}$$

where $\mathbf{r}$ and $\mathbf{v}$ are the J2000 position and velocity vectors. Furthermore let $d\mathbf{x}_f^+$ be the total state differential at t_f following $\Delta \mathbf{x}_f$. The goal of this sub-section is to express $d\mathbf{x}_f^+$ as a function of the independent variables dt_0, $d\mathbf{x}_0^-$, $d(\Delta \mathbf{x}_0)$, dt_f, and $d(\Delta \mathbf{x}_f)$. The final result for $d\mathbf{x}_f^+$ is used repeatedly in the next section to develop state partial derivatives for a notional set of ISS trajectory events.

Begin by noting that the time-fixed variations $\delta \mathbf{x}_f^-$ and $\delta \mathbf{x}_0^+$ are related through the state transition matrix (STM) $\Phi(t_f, t_0)$, abbreviated as $\Phi_{f,0}$, through

$$\delta \mathbf{x}_f^- = \Phi_{f,0} \, \delta \mathbf{x}_0^+. \tag{4}$$

Next note that the plus and minus states at t_0 and t_f are related through $\Delta \mathbf{x}_0$ and $\Delta \mathbf{x}_f$, and also lead to the following total differential expressions for $d\mathbf{x}_0^+$ and $d\mathbf{x}_f^+$.

$$\mathbf{x}_0^+ = \mathbf{x}_0^- + \Delta \mathbf{x}_0 \quad \Rightarrow \quad d\mathbf{x}_0^+ = d\mathbf{x}_0^- + d(\Delta \mathbf{x}_0) \tag{5}$$

$$\mathbf{x}_f^+ = \mathbf{x}_f^- + \Delta \mathbf{x}_f \quad \Rightarrow \quad d\mathbf{x}_f^+ = d\mathbf{x}_f^- + d(\Delta \mathbf{x}_f) \tag{6}$$
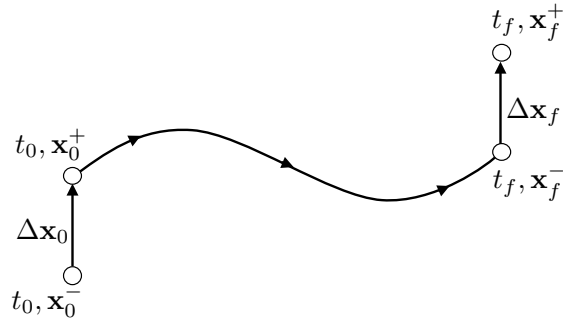
3

Figure 2: Generic Trajectory Segment, as depicted by Ocampo and Munoz.[2] The state $\mathbf{x}$ evolves as: $\left(t_0, \mathbf{x}_0^-\right) \to \Delta\mathbf{x}_0 \to \left(t_0, \mathbf{x}_0^+\right) \to \left(t_f, \mathbf{x}_f^-\right) \to \Delta\mathbf{x}_f \to \left(t_f, \mathbf{x}_f^+\right)$

The total differentials $d\mathbf{x}_f^-$ and $d\mathbf{x}_0^+$ are also related to their respective time-fixed variations through

$$d\mathbf{x}_f^- = \delta\mathbf{x}_f^- + \dot{\mathbf{x}}_f^- dt_f \tag{7}$$

$$d\mathbf{x}_0^+ = \delta\mathbf{x}_0^+ + \dot{\mathbf{x}}_0^+ dt_0 \quad \Rightarrow \quad \delta\mathbf{x}_0^+ = d\mathbf{x}_0^+ - \dot{\mathbf{x}}_0^+ dt_0. \tag{8}$$

Using Equations 4 through 8, it is readily shown that

$$d\mathbf{x}_f^+ = \Phi_{f,0}\left[d\mathbf{x}_0^- - \dot{\mathbf{x}}_0^+ dt_0 + d\left(\Delta\mathbf{x}_0\right)\right] + \dot{\mathbf{x}}_f^- dt_f + d\left(\Delta\mathbf{x}_f\right). \tag{9}$$

which is the desired result in terms of the independent variables. Ultimately though, the *real* independent variables, or controls, in this problem are the burn Δv magnitudes as noted previously. The quantities $\Delta\mathbf{x}_0$ and $\Delta\mathbf{x}_f$ in Equation 9 therefore become dependent variables, themselves functions of the burn Δv magnitudes. This effect is addressed in the next section on state partial derivatives.

State Partial Derivatives

The state partial derivatives are best related by examining a notional set of ISS trajectory events, as shown in Figure 3. This figure depicts seven trajectory events that occur at times t_1 through t_7, with an initial coast arc that occurs from t_0 to t_1. Reboost burns (Δv) occur at Events 1, 3, and 6, while LAN constraints (λ) occur at Events 2, 4, 5, and 7.

State differentials are now developed, event by event, using Equation 9 as a guide. The state partial derivatives are obtained directly from these expressions and used in the next section to form the desired constraint partial derivatives.

Event 1

Applying Equation 9 to Event 1, and assuming $\mathbf{x}_0$, t_0, and t_1 are fixed, then $d\mathbf{x}_0^- = d\left(\Delta\mathbf{x}_0\right) = \mathbf{0}$, and $dt_0 = dt_1 = 0$, leaving

$$d\mathbf{x}_1^+ = d\left(\Delta\mathbf{x}_1\right). \tag{10}$$

However, as noted in earlier, $\Delta\mathbf{x}_1$ is itself a function of Δv_1, namely

$$\Delta\mathbf{x}_1 = \begin{bmatrix} \mathbf{0}_{3\times 1} \\ \boldsymbol{T}_L^I(\mathbf{r}_1, \mathbf{v}_1^-) \cdot \hat{\mathbf{u}}_1 \, \Delta v_1 \end{bmatrix}, \tag{11}$$
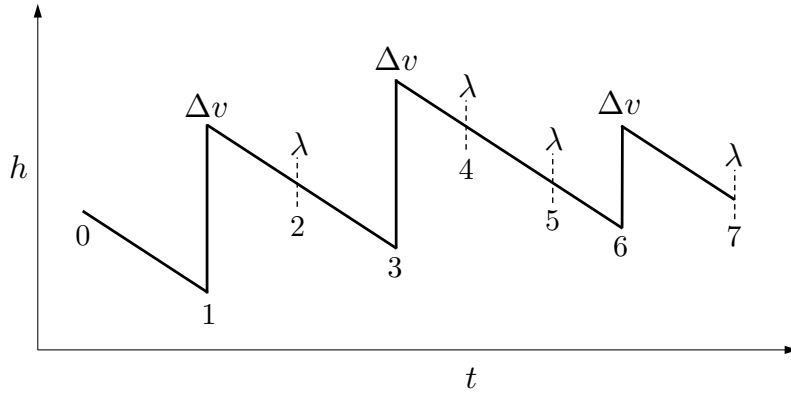
Figure 3: Altitude (h) vs. time (t) for a notional set of seven ISS trajectory events. These events include reboost burns (Δv) and LAN constraints (λ) that must be met by those burns.

where $\boldsymbol{T}_L^I$ is the transformation matrix from the LVLH frame (L) to the J2000 frame (I), and $\hat{\mathbf{u}}_1$ is the $\Delta\mathbf{v}$ unit vector in the LVLH frame defined by ψ_1 and θ_1,

$$\hat{\mathbf{u}}_1 = \begin{bmatrix} \cos\theta_1 \cos\psi_1 & \cos\theta_1 \sin\psi_1 & \sin\theta_1 \end{bmatrix}^T. \tag{12}$$

Equation 10 therefore becomes

$$dx_1^+ = \begin{bmatrix} \mathbf{0}_{3\times1} \\ \boldsymbol{T}_L^I(\mathbf{r}_1, \mathbf{v}_1^-) \cdot \hat{\mathbf{u}}_1 \end{bmatrix} d(\Delta v_1). \tag{13}$$

Event 2

Applying Equation 9 now to Event 2, with $\mathbf{x}_1^-$ and t_1 fixed, and $\Delta\mathbf{x}_2 = \mathbf{0}$,

$$d\mathbf{x}_2 = \Phi_{2,1} \, d(\Delta\mathbf{x}_1) + \dot{\mathbf{x}}_2 \, dt_2. \tag{14}$$

Ignoring the $\dot{\mathbf{x}}_2 \, dt_2$ term for a moment, the rest of Equation 14 takes an arbitrary perturbation in $\Delta\mathbf{x}_1$, i.e. $d(\Delta\mathbf{x}_1)$, and maps it via the STM to the corresponding perturbation in $\mathbf{x}_2$, i.e., $d\mathbf{x}_2$. Now along the nominal, unperturbed trajectory, $\mathbf{x}_2$ occurs at an ascending node, since the LAN constraint at Event 2, by definition, requires evaluating the spacecraft's longitude when it is at the ascending node. Any perturbed trajectory must likewise have its $\mathbf{x}_2$ occurring at the ascending node in order to facilitate an apples-to-apples comparison of LAN values between the perturbed and nominal trajectories.

Now being at the ascending node in both the nominal and perturbed cases requires the z-component of $\mathbf{r}_2$ (i.e. z_2) to be 0 in the True-of-Date (TOD) Earth Equator coordinate system. The TOD system is similar to J2000, but is defined using the true Earth equator and true equinox of date. While the ascending node can be referenced to either J2000 or TOD, the TOD system is used since the LAN by definition is measured along Earth's true equator. The $z_2 = 0$ requirement is already satisfied by definition along the nominal trajectory. Along the perturbed trajectory, however, $d(\Delta\mathbf{x}_1)$ propagated to the same t_2 results in a perturbed $\mathbf{x}_2$ that is no longer at the ascending node, falling above or below the node, depending on the nature of $d(\Delta\mathbf{x}_1)$. Left uncorrected, the perturbed $\mathbf{x}_2$ cannot

5

be compared with the nominal trajectory since it is not at the ascending node, thus leaving the LAN undefined, or at least unknown.

To remedy the situation, the $\dot{\mathbf{x}}_2 \, dt_2$ term is re-introduced and utilized to enforce the $z_2 = 0$ requirement, thereby bringing the perturbed $\mathbf{x}_2$ up to or down to the ascending node as needed. This is accomplished by first expressing the $z_2 = 0$ requirement more formally as

$$z_2 = \mathbf{k}_{\lambda_2}^T \mathbf{x}_2 = 0, \quad \mathbf{k}_{\lambda_2}^T \triangleq \begin{bmatrix} 0 & 0 & 1 & 0 & 0 & 0 \end{bmatrix} \begin{bmatrix} \boldsymbol{T}_{J2K}^{TOD} & \mathbf{0}_{3x3} \\ \mathbf{0}_{3x3} & \boldsymbol{T}_{J2K}^{TOD} \end{bmatrix}, \tag{15}$$

where $\boldsymbol{T}_{J2K}^{TOD}$ is the 3x3 transformation matrix from J2000 to TOD, the λ subscript denotes the $z_2 = 0$ requirement on LAN, and the event number (2) sub-subscript defines the epoch at which $\boldsymbol{T}_{J2K}^{TOD}$ is evaluated. Proceeding,

$$z_2 = \mathbf{k}_{\lambda_2}^T \mathbf{x}_2 = 0 \quad \Rightarrow \quad dz_2 = \mathbf{k}_{\lambda_2}^T d\mathbf{x}_2 = 0, \tag{16}$$

and Equation 14 therefore becomes

$$\mathbf{k}_{\lambda_2}^T d\mathbf{x}_2 = 0 = \mathbf{k}_{\lambda_2}^T \Phi_{2,1} \, d\left(\Delta\mathbf{x}_1\right) + \mathbf{k}_{\lambda_2}^T \dot{\mathbf{x}}_2 \, dt_2. \tag{17}$$

Solving Equation 17 for dt_2,

$$dt_2 = -\frac{\mathbf{k}_{\lambda_2}^T}{\mathbf{k}_{\lambda_2}^T \dot{\mathbf{x}}_2} \Phi_{2,1} \, d\left(\Delta\mathbf{x}_1\right). \tag{18}$$

$d\mathbf{x}_2$ is then found by substituting dt_2 back into Equation 14 to obtain

$$d\mathbf{x}_2 = \left[\mathbf{I}_{6\times6} - \frac{\dot{\mathbf{x}}_2 \mathbf{k}_{\lambda_2}^T}{\mathbf{k}_{\lambda_2}^T \dot{\mathbf{x}}_2} \right] \Phi_{2,1} \, d\left(\Delta\mathbf{x}_1\right). \tag{19}$$

The preceding development is best understood by re-examining Equation 14 in light of the time-fixed variation $\delta\mathbf{x}$,

$$d\mathbf{x}_2 = \delta\mathbf{x}_2 + \dot{\mathbf{x}}_2 \, dt_2, \quad \delta\mathbf{x}_2 = \Phi_{2,1} \, d\left(\Delta\mathbf{x}_1\right), \tag{20}$$

and in conjunction with Figure 4. This figure shows a nominal trajectory that stops at the ascending node and a perturbed trajectory that stops above the ascending node, both at time t_2. The quantity $\delta\mathbf{x}_2$ represents the time-fixed variation in $\mathbf{x}_2$. The quantity dt_2 then represents a time slip in t_2, computed such that $d\mathbf{x}_2 = \delta\mathbf{x}_2 + \dot{\mathbf{x}}_2 \, dt_2$ lies along the TOD equator, thus satisfying the $dz_2 = 0$ requirement. This process is dubbed "ascending node shaping," since it takes an $\mathbf{x}_2$ that is initially dispersed in all six components, and flattens the dispersion such that $d\mathbf{x}_2$ lies along the TOD equator. As mentioned earlier, this shaping is necessary in order to properly compare LAN values between the perturbed and nominal trajectories.

Defining the following shaping matrices,

$$\boldsymbol{S}_{t_2}^{\lambda} \triangleq -\frac{\mathbf{k}_{\lambda_2}^T}{\mathbf{k}_{\lambda_2}^T \dot{\mathbf{x}}_2} \quad \text{and} \quad \boldsymbol{S}_{\mathbf{x}_2}^{\lambda} \triangleq \left[\mathbf{I}_{6\times6} - \frac{\dot{\mathbf{x}}_2 \mathbf{k}_{\lambda_2}^T}{\mathbf{k}_{\lambda_2}^T \dot{\mathbf{x}}_2} \right], \tag{21}$$
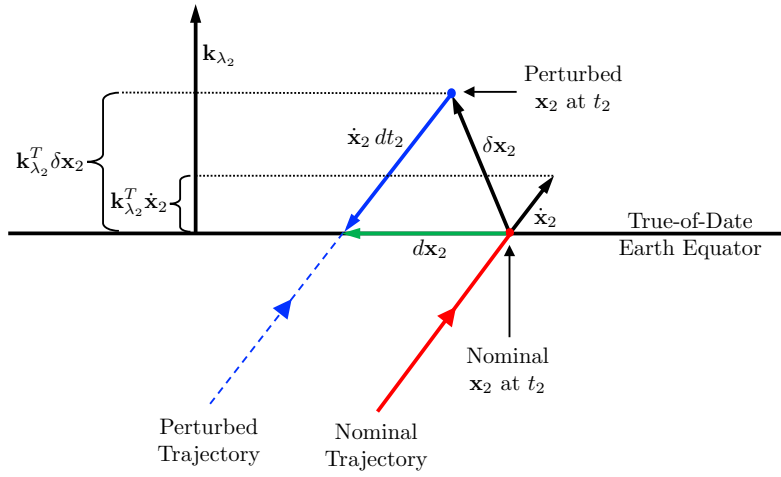
6

Figure 4: Ascending Node Shaping

Equations 18 and 19 become

$$dt_2 = \boldsymbol{S}_{t_2}^{\lambda} \Phi_{2,1} \, d \left(\Delta \mathbf{x}_1 \right) \tag{22}$$

$$d\mathbf{x}_2 = \boldsymbol{S}_{\mathbf{x}_2}^{\lambda} \Phi_{2,1} \, d \left(\Delta \mathbf{x}_1 \right). \tag{23}$$

The terms "time slip" and "shaping matrix" are borrowed from Moesser,[3] who uses Equations 18 and 19 in the context of linear covariance analysis to examine the Lunar powered descent problem. Moesser further notes that $\boldsymbol{S}_{\mathbf{x}_2}^{\lambda}$ is an idempotent shaping matrix, which exhibits the property

$$\left(\boldsymbol{S}_{\mathbf{x}_2}^{\lambda} \right)^2 = \boldsymbol{S}_{\mathbf{x}_2}^{\lambda} \boldsymbol{S}_{\mathbf{x}_2}^{\lambda} = \boldsymbol{S}_{\mathbf{x}_2}^{\lambda}. \tag{24}$$

Another property worth noting is that $\boldsymbol{S}_{\mathbf{x}_2}^{\lambda}$ contains at least one zero eigenvalue and is therefore rank deficient. This can be deduced geometrically by noting that $\boldsymbol{S}_{\mathbf{x}_2}^{\lambda}$ always zeros out (and therefore removes information from) the z-channel by enforcing $z_2 = 0$.

Finally, substituting $\Delta \mathbf{x}_1$ from Equation 11 into Equations 22 and 23 yields

$$dt_2 = \boldsymbol{S}_{t_2}^{\lambda} \Phi_{2,1} \begin{bmatrix} \mathbf{0}_{3 \times 1} \\ \boldsymbol{T}_L^I (\mathbf{r}_1, \mathbf{v}_1^-) \cdot \hat{\mathbf{u}}_1 \end{bmatrix} d \left(\Delta v_1 \right) \tag{25}$$

$$d\mathbf{x}_2 = \boldsymbol{S}_{\mathbf{x}_2}^{\lambda} \Phi_{2,1} \begin{bmatrix} \mathbf{0}_{3 \times 1} \\ \boldsymbol{T}_L^I (\mathbf{r}_1, \mathbf{v}_1^-) \cdot \hat{\mathbf{u}}_1 \end{bmatrix} d \left(\Delta v_1 \right). \tag{26}$$

These expressions can also be written more compactly by utilizing $\delta \mathbf{x}$ in Equation 9 again to yield

$$dt_2 = \boldsymbol{S}_{t_2}^{\lambda} \delta \mathbf{x}_2 \tag{27}$$

$$d\mathbf{x}_2 = \boldsymbol{S}_{\mathbf{x}_2}^{\lambda} \delta \mathbf{x}_2. \tag{28}$$

This form of the time and state differential expressions is useful since it is identical for subsequent events and therefore reduces code complexity.

Event 3

Applying Equation 9 now to Event 3, with $\Delta\mathbf{x}_2 = \mathbf{0}$,

$$d\mathbf{x}_3^+ = \Phi_{3,2}\left[d\mathbf{x}_2 - \dot{\mathbf{x}}_2\,dt_2\right] + \dot{\mathbf{x}}_3^-\,dt_3 + d\left(\Delta\mathbf{x}_3\right). \tag{29}$$

Substituting dt_2 from Equation 18 and $d\mathbf{x}_2$ from Equation 19 into Equation 29 yields

$$d\mathbf{x}_3^+ = \Phi_{3,2}\,\Phi_{2,1}\,d\left(\Delta\mathbf{x}_1\right) + \dot{\mathbf{x}}_3^-\,dt_3 + d\left(\Delta\mathbf{x}_3\right). \tag{30}$$

At this point a similar shaping analysis must be performed for Event 3. This event, a reboost burn, does not occur at an ascending node as in Event 2, but rather at apogee, and is therefore dubbed "apogee shaping." Whereas the requirement by ascending node shaping was $z_2 = 0$ in the TOD system, the analogous requirement by apogee shaping is

$$\cos\gamma_3^- = \mathbf{r}_3^T\mathbf{v}_3^- = 0. \tag{31}$$

This requirement, and the shaping derived from it, ensures that the reboost burn is in fact performed at apogee. Left uncorrected, a perturbed $\mathbf{x}_3^-$ resulting from $d\left(\Delta v_1\right)$ would not be at apogee, and therefore the reboost burn would not occur at apogee as needed. Mathematically, this requirement also holds at perigee. This ambiguity, however, is eschewed by noting that

$$\frac{\partial\left(\mathbf{r}_3^T\mathbf{v}_3^-\right)}{\partial t} = \mathbf{r}_3^T\dot{\mathbf{v}}_3^- + (v_3^-)^2 \tag{32}$$

is negative at apogee and positive at perigee. Proceeding,

$$d(\cos\gamma_3^-) = \mathbf{k}_{\gamma 3}^T\,d\mathbf{x}_3^- = 0, \quad \mathbf{k}_{\gamma 3}^T \triangleq \left[\ (\mathbf{v}_3^-)^T \quad \mathbf{r}_3^T\ \right], \tag{33}$$

where the γ subscript denotes the $\cos\gamma$ requirement at apogee. Returning to Equation 30,

$$d\mathbf{x}_3^+ = d\mathbf{x}_3^- + d\left(\Delta\mathbf{x}_3\right), \quad d\mathbf{x}_3^- = \Phi_{3,2}\,\Phi_{2,1}\,d\left(\Delta\mathbf{x}_1\right) + \dot{\mathbf{x}}_3^-\,dt_3. \tag{34}$$

Therefore,

$$\mathbf{k}_{\gamma 3}^T\,d\mathbf{x}_3^- = 0 = \mathbf{k}_{\gamma 3}^T\Phi_{3,2}\,\Phi_{2,1}\,d\left(\Delta\mathbf{x}_1\right) + \mathbf{k}_{\gamma 3}^T\dot{\mathbf{x}}_3^-\,dt_3. \tag{35}$$

Following a procedure similar to Event 2 results in

$$dt_3 = -\frac{\mathbf{k}_{\gamma 3}^T}{\mathbf{k}_{\gamma 3}^T\dot{\mathbf{x}}_3^-}\,\Phi_{3,2}\,\Phi_{2,1}\,d\left(\Delta\mathbf{x}_1\right) \tag{36}$$

$$d\mathbf{x}_3^- = \left[\mathbf{I}_{6\times6} - \frac{\dot{\mathbf{x}}_3^-\mathbf{k}_{\gamma 3}^T}{\mathbf{k}_{\gamma 3}^T\dot{\mathbf{x}}_3^-}\right]\Phi_{3,2}\,\Phi_{2,1}\,d\left(\Delta\mathbf{x}_1\right). \tag{37}$$

As before, the preceding development is best understood by examining $d\mathbf{x}_3^-$ in Equation 34 in light of $\delta\mathbf{x}$,

$$d\mathbf{x}_3^- = \delta\mathbf{x}_3^- + \dot{\mathbf{x}}_3^-\,dt_3, \quad \delta\mathbf{x}_3^- = \Phi_{3,2}\,\Phi_{2,1}\,d\left(\Delta\mathbf{x}_1\right), \tag{38}$$

and Figures 5 through 7. Figure 5 shows a nominal trajectory that stops at apogee and a perturbed trajectory that considers only position dispersions about apogee, both at time $t_3{}^*$. The quantity $\delta\mathbf{r}_3$ represents the time-fixed variation in $\mathbf{r}_3$, and $\mathbf{r}'_3$ represents $\mathbf{r}_3$ along the perturbed trajectory. The quantity dt_3 then represents a time slip in t_3, computed such that $d\mathbf{r}_3 = \delta\mathbf{r}_3 + \dot{\mathbf{r}}_3^- \, dt_3$ is orthogonal to $\mathbf{v}_3^-$, thus ensuring that $\left(\mathbf{v}_3^-\right)^T d\mathbf{r}_3 = 0$ is satisfied. Figure 6 shows the opposite case, considering only pre-burn velocity dispersions at apogee. dt_3 in this case is the time slip in t_3 required such that $d\mathbf{v}_3^- = \delta\mathbf{v}_3^- + \dot{\mathbf{v}}_3^- \, dt_3$ is orthogonal to $\mathbf{r}_3$, thus ensuring that $(\mathbf{r}_3)^T d\mathbf{v}_3^- = 0$ is satisfied. Finally, Figure 7 shows both position *and* pre-burn velocity dispersions at t_3 resulting from $d\left(\Delta v_1\right)$. dt_3 is now the time slip in t_3 required to ensure $d\left(\mathbf{r}_3^T \mathbf{v}_3^-\right) = 0$ is satisfied. This enables the burn at Event 3 to be performed at apogee along the perturbed trajectory (denoted by $\left(\mathbf{r}'_3\right)_a$ and $\left(\mathbf{v}_3'^-\right)_a$ in Figure 7), as desired.
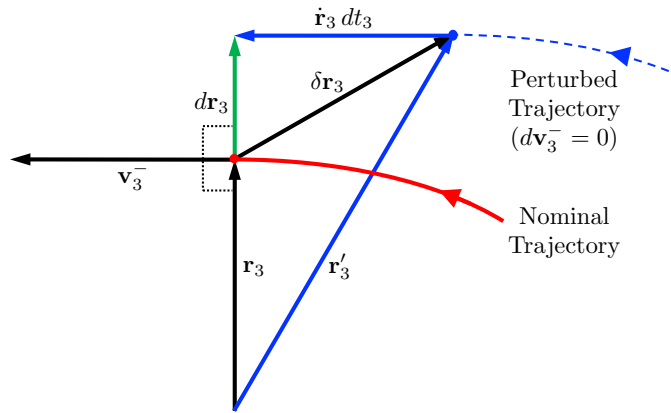

Figure 5: Apogee Shaping, Considering Position Dispersions
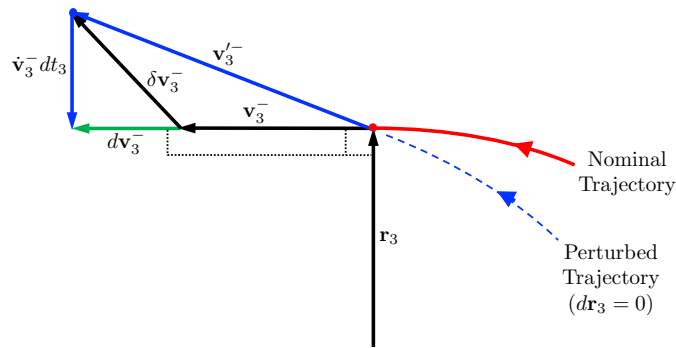

Figure 6: Apogee Shaping, Considering Pre-Burn Velocity Dispersions

---

*Note that this is a fictitious perturbed trajectory, since a perturbation in Δv_1, $d\left(\Delta v_1\right)$, would result in both position *and* pre-burn velocity dispersions at t_3, as shown in Figure 7. Considering these two dispersions separately, however, aids in understanding the mechanism of apogee shaping in the combined dispersion case.
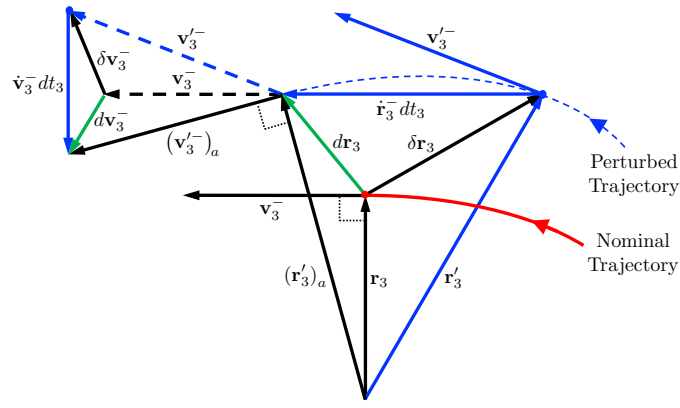
Figure 7: Apogee Shaping, Considering Position and Pre-Burn Velocity Dispersions

Defining shaping matrices similar to Event 2,[*]

$$M_{t_3}^\gamma \triangleq -\frac{\mathbf{k}_{\gamma_3}^T}{\mathbf{k}_{\gamma_3}^T \dot{\mathbf{x}}_3^-} \quad \text{and} \quad M_{\mathbf{x}_3}^\gamma \triangleq \left[\mathbf{I}_{6\times 6} - \frac{\dot{\mathbf{x}}_3^- \mathbf{k}_{\gamma_3}^T}{\mathbf{k}_{\gamma_3}^T \dot{\mathbf{x}}_3^-} \right],$$

(39)

Equations 36 and 37 become

$$dt_3 = M_{t_3}^\gamma \Phi_{3,2}\, \Phi_{2,1}\, d\left(\Delta \mathbf{x}_1\right)$$

(40)

$$d\mathbf{x}_3^- = M_{\mathbf{x}_3}^\gamma \Phi_{3,2}\, \Phi_{2,1}\, d\left(\Delta \mathbf{x}_1\right).$$

(41)

And again, substituting $\Delta \mathbf{x}_1$ from Equation 11 yields

$$dt_3 = M_{t_3}^\gamma \Phi_{3,2}\, \Phi_{2,1} \left[\begin{array}{c} \mathbf{0}_{3\times 1} \\ \boldsymbol{T}_L^I(\mathbf{r}_1, \mathbf{v}_1^-) \cdot \hat{\mathbf{u}}_1 \end{array} \right] d\left(\Delta v_1\right)$$

(42)

$$d\mathbf{x}_3^- = M_{\mathbf{x}_3}^\gamma \Phi_{3,2}\, \Phi_{2,1} \left[\begin{array}{c} \mathbf{0}_{3\times 1} \\ \boldsymbol{T}_L^I(\mathbf{r}_1, \mathbf{v}_1^-) \cdot \hat{\mathbf{u}}_1 \end{array} \right] d\left(\Delta v_1\right).$$

(43)

Similar to Equations 27 and 28 for Event 2, Equations 42 and 43 can be formulated as

$$dt_3 = M_{t_3}^\gamma \delta \mathbf{x}_3^-$$

(44)

$$d\mathbf{x}_3^- = M_{\mathbf{x}_3}^\gamma \delta \mathbf{x}_3^-.$$

(45)

Returning to Equation 34,

$$d\mathbf{x}_3^+ = d\mathbf{x}_3^- + d\left(\Delta \mathbf{x}_3\right).$$

(46)

---

[*]M^γ is used here for the apogee shaping matrix instead of $\boldsymbol{S}^\gamma$ because the apogee shaping matrix for the state takes one form (defined by $M_{\mathbf{x}}^\gamma$) when examining the burn event itself, and a different form (defined by $\boldsymbol{S}_{\mathbf{x}}^\gamma$) when examining a downstream event, such as Event 4.

The quantity $d(\Delta \mathbf{x}_3)$, however, is a function of $d(\Delta v_1)$ and $d(\Delta v_3)$. Therefore,

$$d\mathbf{x}_3^+ = \frac{\partial \mathbf{x}_3^-}{\partial (\Delta v_1)} d(\Delta v_1) + \frac{\partial (\Delta \mathbf{x}_3)}{\partial (\Delta v_1)} d(\Delta v_1) + \frac{\partial (\Delta \mathbf{x}_3)}{\partial (\Delta v_3)} d(\Delta v_3) \qquad (47)$$

$$= \underbrace{\left[\mathbf{I}_{6\times6} + \frac{\partial (\Delta \mathbf{x}_3)}{\partial \mathbf{x}_3^-} \right] \frac{\partial (\mathbf{x}_3^-)}{\partial (\Delta v_1)} d(\Delta v_1)}_{A} + \underbrace{\frac{\partial (\Delta \mathbf{x}_3)}{\partial (\Delta v_3)} d(\Delta v_3)}_{B}. \qquad (48)$$

Before proceeding, it is worthwhile to understand the physical effects of $d(\Delta v_1)$ and $d(\Delta v_3)$ on $d(\Delta \mathbf{x}_3)$. B is the more obvious effect, representing the change in $\Delta \mathbf{x}_3$ due to a change in Δv_3. A, in contrast, represents the change in $\Delta \mathbf{x}_3$ due to a change in Δv_1, even if Δv_3 is zero. This is because a change in Δv_1 causes a change in the inertial location of apogee at Event 3, thus changing the LVLH frame at Event 3. Since all burns are expressed in the LVLH frame, a change in the LVLH frame translates to a change in the inertial burn $\Delta \mathbf{v}$, and therefore a change to $\Delta \mathbf{x}_3$.

Returning to Equation 48,

$$\frac{\partial (\Delta \mathbf{x}_3)}{\partial (\Delta v_3)} = \begin{bmatrix} \mathbf{0}_{3\times1} \\ \boldsymbol{T}_L^I(\mathbf{r}_3, \mathbf{v}_3^-) \cdot \hat{\mathbf{u}}_3 \end{bmatrix} \qquad (49)$$

$$\frac{\partial \mathbf{x}_3^-}{\partial (\Delta v_1)} = \boldsymbol{M}_{\mathbf{x}_3}^\gamma \Phi_{3,2} \, \Phi_{2,1} \begin{bmatrix} \mathbf{0}_{3\times1} \\ \boldsymbol{T}_L^I(\mathbf{r}_1, \mathbf{v}_1^-) \cdot \hat{\mathbf{u}}_1 \end{bmatrix}, \qquad (50)$$

and the only unknown partial now is $\partial (\Delta \mathbf{x}_3)/\partial \mathbf{x}_3^-$. To obtain this partial, first note that

$$\frac{\partial (\Delta \mathbf{x}_3)}{\partial \mathbf{x}_3^-} = \frac{\partial}{\partial \mathbf{x}_3^-} \begin{bmatrix} \mathbf{0}_{3\times1} \\ \boldsymbol{T}_L^I(\mathbf{r}_3, \mathbf{v}_3^-) \cdot \hat{\mathbf{u}}_3 \, \Delta v_3 \end{bmatrix} = \frac{\partial}{\partial \mathbf{x}_3^-} \begin{bmatrix} \mathbf{0}_{3\times1} \\ \boldsymbol{T}_3 \, (\Delta v_3)_L \end{bmatrix}, \qquad (51)$$

$\boldsymbol{T}_3$ itself is given by

$$\boldsymbol{T}_3 = \begin{bmatrix} (\mathbf{h}_3^- \hat{\times} \mathbf{r}_3) & -\hat{\mathbf{h}}_3^- & -\hat{\mathbf{r}}_3 \end{bmatrix}, \qquad (52)$$

where $\mathbf{h}_3^- = \mathbf{r}_3 \times \mathbf{v}_3^-$ is the pre-burn instantaneous angular momentum vector of the orbit. This form of the transformation matrix can be deduced from Figure 1. Temporarily dropping the 3 subscript, the non-trivial derivative in Equation 51 is

$$\frac{\partial (\boldsymbol{T}(\Delta \mathbf{v})_L)}{\partial \mathbf{x}^-} = \frac{\partial (\mathbf{h}^- \hat{\times} \mathbf{r})}{\partial \mathbf{x}^-} (\Delta \mathbf{v}_x)_L - \frac{\partial \hat{\mathbf{h}}^-}{\partial \mathbf{x}^-} (\Delta \mathbf{v}_y)_L - \frac{\partial \hat{\mathbf{r}}}{\partial \mathbf{x}^-} (\Delta \mathbf{v}_z)_L. \qquad (53)$$

The $(\Delta \mathbf{v})_L$ components are outside the partial derivative since $(\Delta \mathbf{v})_L$ is not a function of $\mathbf{x}^-$. Recalling that

$$\mathbf{x}^- = \begin{bmatrix} \mathbf{r}^T & (\mathbf{v}^-)^T \end{bmatrix}^T, \qquad (54)$$

the three partial derivatives on the right-hand side of Equation 53 are given by

$$\frac{\partial \hat{\mathbf{b}}^-}{\partial \mathbf{x}^-} = \frac{1}{|\mathbf{b}^-|} \left(\mathbf{I}_{3\times3} - \frac{\mathbf{b}^- \mathbf{b}^{-T}}{|\mathbf{b}^-|^2} \right) \begin{bmatrix} [\mathbf{h}^- \times] + [\mathbf{r} \times][\mathbf{v}^- \times] & -[\mathbf{r} \times]^2 \end{bmatrix} \qquad (55)$$

$$\frac{\partial \hat{\mathbf{h}}^-}{\partial \mathbf{x}^-} = \frac{1}{|\mathbf{h}^-|}\left(\mathbf{I}_{3\times3} - \frac{\mathbf{h}^-\mathbf{h}^{-T}}{|\mathbf{h}^-|^2}\right)\left[\begin{array}{c|c} -[\mathbf{v}^-\times] & [\mathbf{r}\times] \end{array}\right] \tag{56}$$

$$\frac{\partial \hat{\mathbf{r}}}{\partial \mathbf{x}^-} = \frac{1}{r}\left(\mathbf{I}_{3\times3} - \frac{\mathbf{r}\,\mathbf{r}^T}{r^2}\right)\left[\begin{array}{c|c} \mathbf{I}_{3\times3} & \mathbf{0}_{3\times3} \end{array}\right], \tag{57}$$

where $\mathbf{b}^- \triangleq \mathbf{h}^- \times \mathbf{r}$ and $[\mathbf{a}\times]$ ($\mathbf{a}$ is $\mathbf{r}$, $\mathbf{v}$, or $\mathbf{h}^-$) is the cross product matrix

$$[\mathbf{a}\times] = \begin{bmatrix} 0 & -a_3 & a_2 \\ a_3 & 0 & -a_1 \\ -a_2 & a_1 & 0 \end{bmatrix}. \tag{58}$$

Therefore,

$$\frac{\partial(\Delta\mathbf{x}_3)}{\partial\mathbf{x}_3^-} = \begin{bmatrix} \mathbf{0}_{3\times6} \\ \dfrac{\partial\hat{\mathbf{b}}_3^-}{\partial\mathbf{x}_3^-}(\Delta\mathbf{v}_{3_x})_L - \dfrac{\partial\hat{\mathbf{h}}_3^-}{\partial\mathbf{x}_3^-}(\Delta\mathbf{v}_{3_y})_L - \dfrac{\partial\hat{\mathbf{r}}_3}{\partial\mathbf{x}_3^-}(\Delta\mathbf{v}_{3_z})_L \end{bmatrix}. \tag{59}$$

Events 4 through 7

Events 4 through 7 work in much the same way, using the concepts and equations developed for Events 1 through 4. The result for Event 7 is

$$d\mathbf{x}_7 = \mathbf{S}_{\mathbf{x}_7}^\lambda \delta\mathbf{x}_7, \tag{60}$$

where

$$
\begin{aligned}
\delta\mathbf{x}_7 = &\left[\left(\mathbf{\Phi}_{7,6}\,\mathbf{S}_{\mathbf{x}_6}^\gamma\right)\left(\mathbf{\Phi}_{6,3}\,\mathbf{S}_{\mathbf{x}_3}^\gamma\right)\mathbf{\Phi}_{3,1}\frac{\partial(\Delta\mathbf{x}_1)}{\partial(\Delta v_1)} + \right.\\
&\left.\left(\mathbf{\Phi}_{7,6}\,\mathbf{S}_{\mathbf{x}_6}^\gamma\right)\mathbf{\Phi}_{6,3}\frac{\partial(\Delta\mathbf{x}_3)}{\partial\mathbf{x}_3^-}\frac{\partial(\mathbf{x}_3^-)}{\partial(\Delta v_1)} + \mathbf{\Phi}_{7,6}\frac{\partial(\Delta\mathbf{x}_6)}{\partial\mathbf{x}_6^-}\frac{\partial(\mathbf{x}_6^-)}{\partial(\Delta v_1)}\right]d(\Delta v_1) + \\
&\left[\left(\mathbf{\Phi}_{7,6}\,\mathbf{S}_{\mathbf{x}_6}^\gamma\right)\mathbf{\Phi}_{6,3}\frac{\partial(\Delta\mathbf{x}_3)}{\partial(\Delta v_3)} + \mathbf{\Phi}_{7,6}\frac{\partial(\Delta\mathbf{x}_6)}{\partial\mathbf{x}_6^-}\frac{\partial(\mathbf{x}_6^-)}{\partial(\Delta v_3)}\right]d(\Delta v_3) + \\
&\left[\mathbf{\Phi}_{7,6}\frac{\partial(\Delta\mathbf{x}_6)}{\partial(\Delta v_6)}\right]d(\Delta v_6),
\end{aligned}
\tag{61}
$$

and $\mathbf{S}_{\mathbf{x}_k}^\gamma$ is defined by

$$\mathbf{S}_{\mathbf{x}_k}^\gamma \triangleq \left[\mathbf{I}_{6\times6} + \frac{(\dot{\mathbf{x}}_k^+ - \dot{\mathbf{x}}_k^-)\,\mathbf{k}_{\gamma_k}^T}{\mathbf{k}_{\gamma_k}^T\dot{\mathbf{x}}_k^-}\right], \quad k = 3, 6. \tag{62}$$

The apogee shaping matrix $\mathbf{S}_{\mathbf{x}}^\gamma$ is different from $M_{\mathbf{x}}^\gamma$ discussed in Event 3, thus requiring a change in notation. In the case of Event 3, this difference emerges from the fact that $d\mathbf{x}_3^+$ (and therefore $M_{\mathbf{x}_3}^\gamma$) is not a function of $\dot{\mathbf{x}}_3^+$, whereas $d\mathbf{x}_4$ (and therefore $\mathbf{S}_{\mathbf{x}_3}^\gamma$) is a function of $\dot{\mathbf{x}}_3^+$. In order to arrive at Event 4, first a time slip in t_3 must be applied in order for the burn at Event 3 to occur at apogee, as discussed previously. If the trajectory simply stopped there, no further action would be required and $M_{\mathbf{x}_3}^\gamma$ would be sufficient. To move forward from Event 3, however, dt_3, must effectively be undone in order to maintain time coherence from Event 3 to Event 4.

Event k

Equations 60 and 61 can be generalized to determine the state differential at an arbitrary Event k. Assume there are n burns prior to t_k. The ith burn ($i = 1, \ldots, n$) occurs at $t_{f(i)} < t_k$, where $f(i)$ is the event number on which burn i occurs. Using the above example, with $n = 3$ and $k = 7$, the burns $i = 1, 2, 3$ occur at events $f(i) = 1, 3, 6$, respectively. If Event k has a constraint, then

$$dt_k = \boldsymbol{S}_{t_k}^{\lambda} \delta \mathbf{x}_k \tag{63}$$

$$d\mathbf{x}_k = \boldsymbol{S}_{\mathbf{x}_k}^{\lambda} \delta \mathbf{x}_k, \tag{64}$$

where $\delta \mathbf{x}_k$ is a lengthy expression that is omitted for brevity. The general pattern of $\delta \mathbf{x}_k$, however, can be inferred from Equation 61.

Constraint Partial Derivatives

The analysis now turns to the LAN and SMA altitude constraint partial derivatives, which require the state partial derivatives developed in the previous section. The goal is to develop the partial derivatives of LAN and SMA altitude with respect to the burn Δv magnitudes.

LAN (λ) is a function of position in the TOD frame ($\mathbf{r}_{TOD}$) and time (t). Temporarily dropping the TOD subscript for notational simplicity, the x and y components of $\mathbf{r}$ in the TOD frame are

$$x = r \cos \phi \cos \theta_L \tag{65}$$

$$y = r \cos \phi \sin \theta_L, \tag{66}$$

where ϕ is the geocentric latitude and θ_L is the local sidereal time. θ_L in turn is given by

$$\theta_L = \theta_G + \lambda, \tag{67}$$

where θ_G is the Greenwich mean sidereal time and λ is the longitude. Without loss of generality, set $\phi = 0$ since λ is not a function of ϕ. The partial derivatives of λ with respect to x and y are then

$$\frac{\partial \lambda}{\partial x} = -\frac{y}{r^2} \quad \text{and} \quad \frac{\partial \lambda}{\partial y} = \frac{x}{r^2}. \tag{68}$$

Resuming the TOD notation,

$$\frac{\partial \lambda}{\partial \mathbf{x}_{TOD}} = \left[\begin{array}{cc} \frac{\partial \lambda}{\partial \mathbf{r}_{TOD}} & \frac{\partial \lambda}{\partial \mathbf{v}_{TOD}} \end{array} \right] = \frac{1}{r^2} \left[\begin{array}{ccccc} -y_{TOD} & x_{TOD} & 0 & 0 & 0 & 0 \end{array} \right]. \tag{69}$$

Therefore,

$$\frac{\partial \lambda}{\partial \mathbf{x}} = \mathbf{m}_{\lambda}^{T} \triangleq \frac{1}{r^2} \left[\begin{array}{ccccc} -y_{TOD} & x_{TOD} & 0 & 0 & 0 & 0 \end{array} \right] \left[\begin{array}{cc} \boldsymbol{T}_{J2K}^{TOD} & \mathbf{0}_{3\times 3} \\ \mathbf{0}_{3\times 3} & \boldsymbol{T}_{J2K}^{TOD} \end{array} \right]. \tag{70}$$

Returning to Equation 67,

$$\lambda = \theta_L - \theta_G = \theta_L - \omega_E (t - t_0) - \theta_{G_0}, \tag{71}$$

where ω_E is the magnitude of Earth's rotation rate in rad/sec, t_0 is an arbitrary reference time, and θ_{G_0} is the value of θ_G at t_0. Therefore,

$$\frac{\partial \lambda}{\partial t} = -\omega_E. \tag{72}$$

Using the chain rule, the total differential of λ at Event k is

$$d\lambda_k = \frac{\partial \lambda_k}{\partial \mathbf{x}_k} d\mathbf{x}_k + \frac{\partial \lambda_k}{\partial t_k} dt_k = \left[\mathbf{m}_{\lambda_k}^T \mathbf{S}_{\mathbf{x}_k}^{\lambda} - \omega_E \, \mathbf{S}_{t_k}^{\lambda} \right] \delta \mathbf{x}_k, \tag{73}$$

from which the partial derivatives for $\partial \lambda_k / \partial \left(\Delta v_{f(i)} \right)$ can be obtained.

SMA altitude, in contrast, is given by $a - R_e$. Beginning with the vis-viva equation,

$$\frac{v^2}{2} - \frac{\mu}{r} = -\frac{\mu}{2a}, \tag{74}$$

it is straight forward to show that

$$\frac{\partial a}{\partial \mathbf{x}} = \mathbf{m}_a^T \triangleq 2a^2 \left[\begin{array}{cc} \frac{1}{r^3} \mathbf{r}^T & \frac{1}{\mu} \mathbf{v}^T \end{array} \right]. \tag{75}$$

Since SMA altitude constraints do not need to occur at a condition such as the ascending node or apogee, no shaping of the state dispersions about a nominal trajectory is required. Therefore $d\mathbf{x}_k = \delta \mathbf{x}_k$ for SMA altitude constraints, and the total differential of a at Event k is

$$da_k = \frac{\partial a_k}{\partial \mathbf{x}_k} d\mathbf{x}_k = \mathbf{m}_{a_k}^T \delta \mathbf{x}_k, \tag{76}$$

from which the partial derivatives for $\partial a_k / \partial \left(\Delta v_{f(i)} \right)$ can be obtained. Note that this formulation assumes an *osculating* or Keplerian value for SMA. In practice however, the ISS trajectory is planned using a *mean* value for SMA, given by

$$\bar{a} = p - \frac{3}{2} J_2 \frac{R_e^2}{p} \left[1 - \frac{3}{2} \sin^2 i + \sin^2 i \cos 2u \right], \tag{77}$$

where $p = a(1 - e^2)$ is the semi-parameter and u is the argument of latitude. Equation 77 comes from internal TOPO documentation and is stated here without attempt to verify its pedigree. The partial derivative of $\bar{a}$ with respect to $\mathbf{x}$ is is given by

$$\frac{\partial \bar{a}}{\partial \mathbf{x}} = \mathbf{m}_{\bar{a}}^T \triangleq \frac{\partial \bar{a}}{\partial p} \left[\frac{\partial p}{\partial a} \frac{\partial a}{\partial \mathbf{x}} + \frac{\partial p}{\partial e} \frac{\partial e}{\partial \mathbf{x}} \right] + \frac{\partial \bar{a}}{\partial i} \frac{\partial i}{\partial \mathbf{x}} + \frac{\partial \bar{a}}{\partial u} \frac{\partial u}{\partial \mathbf{x}}, \tag{78}$$

where the partial derivatives on the right-hand side of Equation 78 have been omitted for brevity. Similar to osculating SMA, the total differential of $\bar{a}$ at Event k is

$$d\bar{a}_k = \frac{\partial \bar{a}_k}{\partial \mathbf{x}_k} d\mathbf{x}_k = \mathbf{m}_{\bar{a}_k}^T \delta \mathbf{x}_k \tag{79}$$

from which the partial derivatives $\partial \bar{a}_k / \partial \left(\Delta v_{f(i)} \right)$ can be obtained.

The preceding developments for λ, a, and $\bar{a}$ can be extended to other constraint functions as needed. Assume c is a generic, scalar constraint function at Event k of the form

$$c_k = f(\mathbf{x}_k, t_k). \tag{80}$$

If c_k is differentiable with respect to both $\mathbf{x}$ and t, then

$$dc_k = \left[\frac{\partial c_k}{\partial \mathbf{x}_k} \mathbf{S}_{\mathbf{x}_k}^c + \frac{\partial c_k}{\partial t_k} \mathbf{S}_{t_k}^c \right] \delta \mathbf{x}_k, \tag{81}$$

from which the partial derivatives $\partial c_k / \partial \left(\Delta v_{f(i)} \right)$ can be obtained. In this expression, $\mathbf{S}_{\mathbf{x}_k}^c$ and $\mathbf{S}_{t_k}^c$ are the appropriate state and time shaping matrices for c_k, respectively. These matrices may be identity, zero, or non-trivial depending on the nature of c_k.

REAL-WORLD ISS PROBLEMS AND RESULTS

The above framework is now used to analyze two ISS trajectory event sequences. For each sequence, the ISS trajectory is numerically integrated from event to event using FreeFlyer v7.2.1.37946 under the following assumptions.

- Force model: Non-spherical Earth gravity (EGM-96 7x7), Sun and Moon point mass gravity (DE430), and atmospheric drag (analytic density model, based on a constant temperature hydrostatic model).

- Docking and undocking events are ignored, and the ISS total mass, coefficient of drag (Cd), and drag area are fixed to constant values.

- All burns are assumed to have yaw = pitch = $0°$.

FreeFlyer numerically integrates the six-element state (position and velocity) along with the thirty-six element STM from event to event, saving off the state, STM, and other necessary results at each event. After reaching t_f, a FreeFlyer script performs chain rule operations on the saved results in order to form the constraint gradients. Given the time frames spanned by ISS look-ahead trajectory plans—six weeks to roughly two years—obtaining the constraint gradients in this manner (via single propagation from t_0 to t_f) is generally more efficient than using finite differences.

This entire integration process can be thought of as a black box, which is called by MATLAB's *fmincon* function to solve the constrained burn optimization problem. *fmincon* begins with an initial estimate of the Δv values (discussed further below), which are the controls in the optimization problem. At each iteration, MATLAB sends the current Δv values to FreeFlyer, which in turn updates the event sequence with these values, re-integrates the ISS trajectory from t_0 to t_f, computes the constraint gradients at t_f, and returns the results to MATLAB. *fmincon* then uses these gradients along with the objective gradient in Equation 2 to update its estimate of the Δv values. This process repeats until MATLAB converges on a locally-optimal (i.e. minimum total Δv) solution, assuming one exists. A feasible solution—one that simply adjusts the Δv values to meet the constraints—can also be obtained by simply setting $J = 0$ instead of using J from Equation 1.

The first sequence to be analyzed consists of events taken from a TOPO look-ahead plan generated in February, 2016. The relevant events (i.e., those having burns or constraints) are listed in truncated form in Table 1. In this table as well as in Table 2 for the second sequence, "sm" means a reboost performed using the ISS Service Module (SM) main engines, "#s" means a Soyuz event, and "#p" means a Progress event. The initial Δv values in Table 1 are taken directly from the look-ahead plan, while the final Δv values are the optimized values. Figure 8 shows the mean SMA altitude plot using both initial and optimized Δv values. Figures 9 and 10 show the total Δv vs. iteration and the maximum constraint violation vs. total Δv, respectively.

In order to avoid event overlap, the second sequence consists of events from a different TOPO look-ahead plan generated slightly more than a year later, in March, 2017. The table and figures that follow mirror those used in the previous sequence. One difference in this sequence is that the initial Δv values in Table 2 are obtained using rules of thumb that relate Δv to the value of the next downstream constraint. These rules of thumb and their derivation have been omitted for brevity.

Examining the first event sequence, Figure 9 is suspect since the initial estimate, taken directly from the actual look-ahead plan, results in an infeasible point, and the optimal total Δv is in fact higher (8.084 m/s) than the initial total Δv (7.900 m/s). This effect, however, is attributed to differences in force models, propagators, environment parameters (e.g. Earth's rotation rate), event
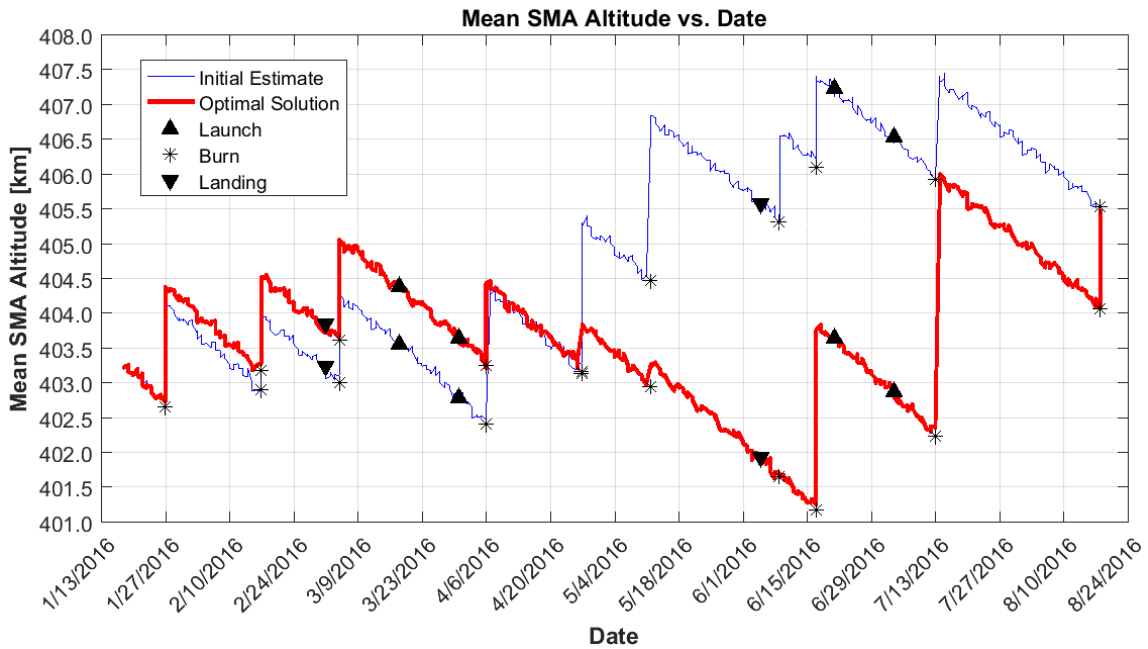
Figure 8: Mean SMA Altitude Plot, February through Mid-August, 2016. The final burn and SMA altitude constraint "normalize" the solution so that both the initial estimate and optimal solution end at the same altitude.
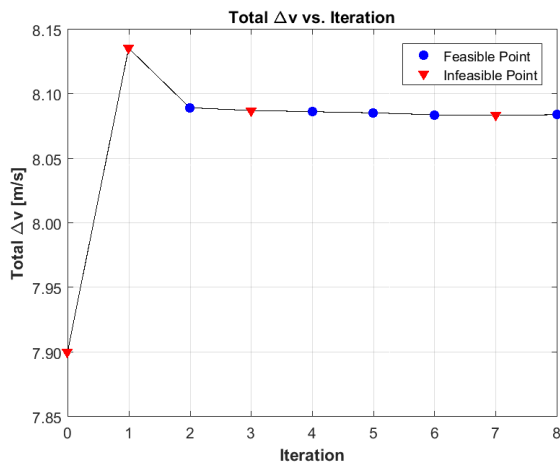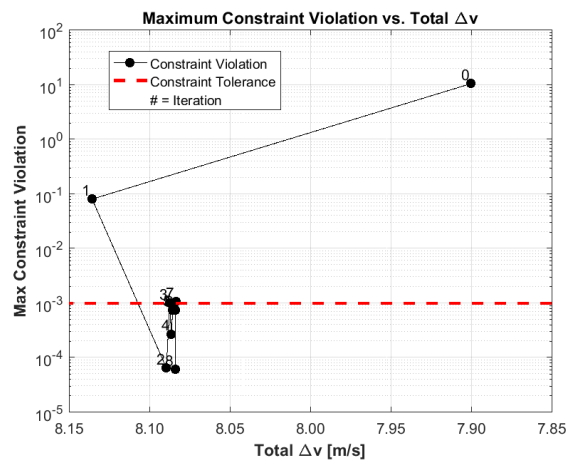

Figure 9: Total Δv vs. Iteration

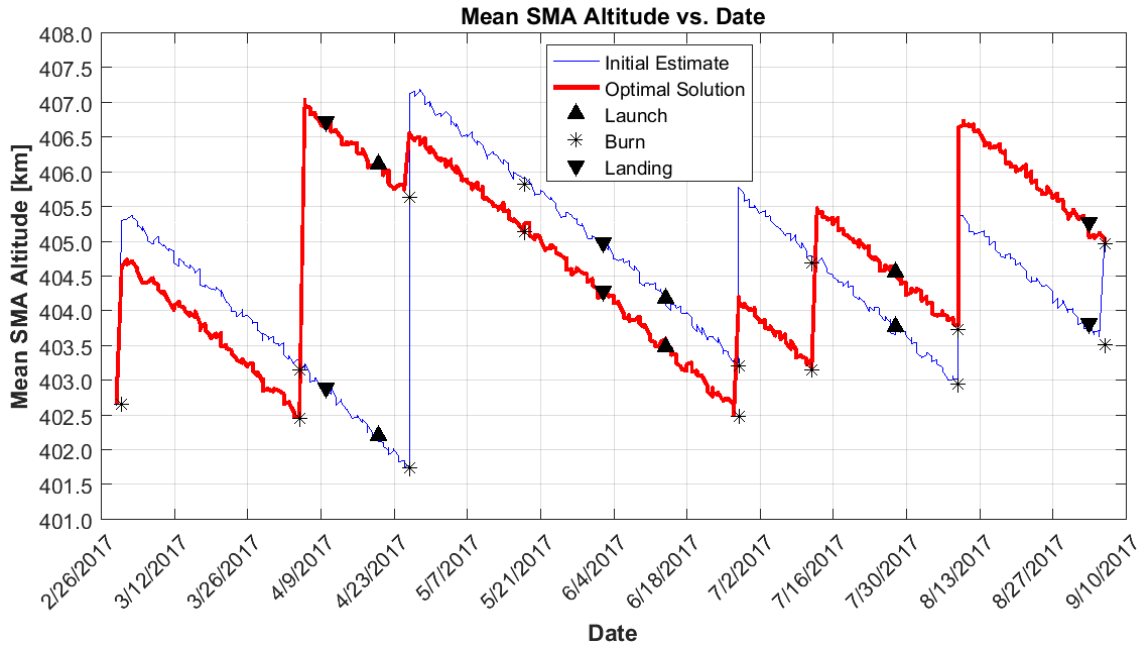**Figure 10**: Max Constraint Violation vs. Δv

Figure 11: Mean SMA Altitude Plot, March through Early September, 2017. Normalized solution.
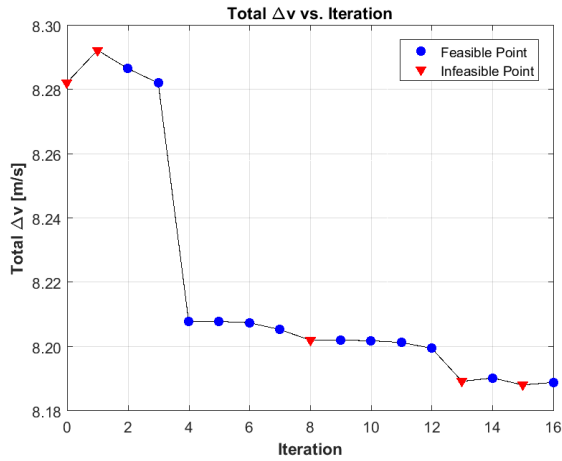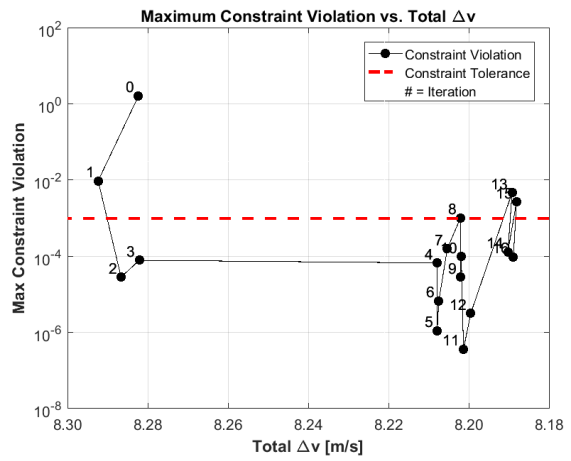

Figure 12: Total Δv vs. Iteration

Figure 13: Max Constraint Violation vs. Δv

17

Table 1: ISS Trajectory Events, February through Mid-August, 2016

Name	Date	Type	Initial Δv (m/s)	Final Δv (m/s)	Min LAN/Alt (deg/km)	Max LAN/Alt (deg/km)
61p_reboost3	01/27/2016	Burn	0.800	0.954		
61p_reboost4	02/17/2016	Burn	0.600	0.772		
44s_landing	03/02/2016	LAN			12.7	16.5
⋮	⋮	⋮	⋮	⋮	⋮	⋮
63p_reboost7	08/18/2016	Burn	0.000	1.794		
SMA_altitude	08/19/2016	Alt			405.5	405.5
		TOTAL	7.900	8.084		

Table 2: ISS Trajectory Events, March through Early September, 2017

Name	Date	Type	Initial Δv (m/s)	Final Δv (m/s)	Min LAN/Alt (deg/km)	Max LAN/Alt (deg/km)
sm_reboost1	03/02/2017	Burn	1.575	1.201		
sm_reboost2	04/05/2017	Burn	0.000	2.539		
48s_landing	04/10/2017	LAN			12.7	16.5
⋮	⋮	⋮	⋮	⋮	⋮	⋮
sm_reboost8	09/05/2017	Burn	0.855	0.000		
SMA_altitude	09/07/2017	Alt			405.0	405.0
		TOTAL	8.282	8.189		

triggers, etc. between this approach and the currently process for creating the trajectory plan. In general, direct comparison between trajectory plans generated using the approach outlined here and those generated using the current process is limited. This is especially so given the multi-month propagations that amplify these differences over time. Notwithstanding, in this case the optimizer takes the initial, infeasible point, and converges on an optimal solution that meets the constraints. The second sequence exhibits similar behavior, starting from an infeasible point and converging on an optimal solution subject to the constraints. However, in this case the optimal solution is at least not *worse* than the initial estimate.

In both sequences, as noted in Figures 8 and 11, the final burn and SMA altitude constraint "normalize" the solution to ensure consistency. Absent this normalization, a lower total Δv solution may be available, but the resulting SMA altitude at t_f will likely also be lower. Since the ISS is continuously subject to atmospheric drag, this reduction in altitude, or equivalently, energy, must be made up at some point in the future, beyond the time horizon being analyzed. Thus any Δv reduction achieved over $[t_0, t_f]$ is arguably only temporary. Normalizing the solution via a final burn and SMA altitude constraint resolves this issue, however when coupled with the tight LAN constraints, it leaves little room for substantive Δv savings.

This being said, a *non*-normalized solution, one that does not have a final burn and SMA altitude

constraint, still has value for trajectory planning. In a situation where it becomes necessary to ration propellant, a non-normalized solution can provide non-trivial Δv savings over a given period of time without considering longer-term altitude degradation. Such a situation is in fact feasible, given that there have been three Progress vehicle failures since 2011, each of which was carrying ISS resupply propellant that was obviously lost with the vehicle. While propellant rationing was not required in these cases, had it been required, a non-normalized minimum Δv solution would provide key information to program managers.

Returning to the March, 2017 event sequence, Figures 14 through 16 show this same sequence, but excluding the final burn and SMA altitude constraint. The optimizer in this case is able to quickly find an optimal solution that meets the constraints, and deliver almost a full 1.5 m/s of Δv savings over the normalized solution. This represents a significant savings, given that a typical six-month plan requires anywhere from 6 to 10 m/s of Δv. These savings, of course, will vary depending on several factors, such as the pedigree of the initial estimate, the number and type of events in the plan, and the plan duration.
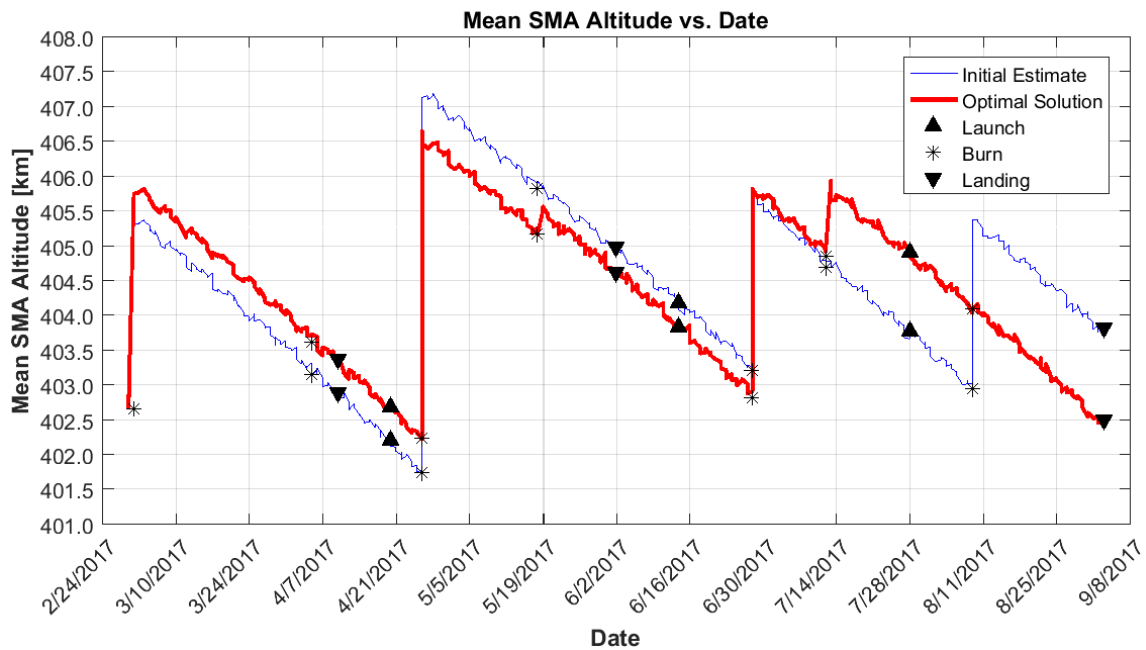

Figure 14: Mean SMA Altitude Plot, March through Early September, 2017. The non-normalized solution and its effect on the trajectory are clearly visible at t_f.

CONCLUSIONS

This work provides a formulation and solution of the constrained burn optimization problem for the ISS. The formulation includes analytic derivatives for the objective function, and variational equations using STMs for the constraint functions. These equations are used in a combined MATLAB-FreeFlyer framework to provide locally-minimal total Δv solutions to real-world ISS burn planning problems.

This framework provides several unique advantages over the current process for obtaining ISS burn solutions. First, it introduces automatic computation of constraint gradients with a single
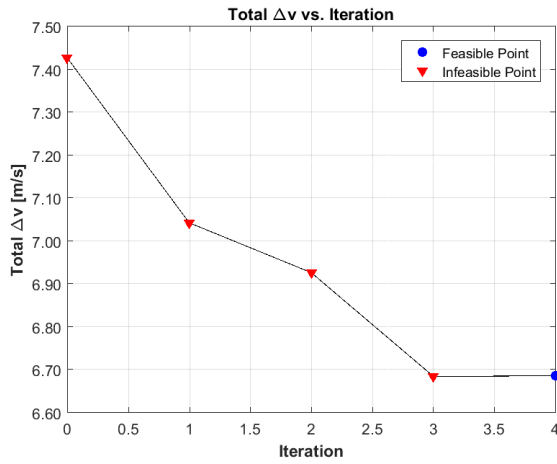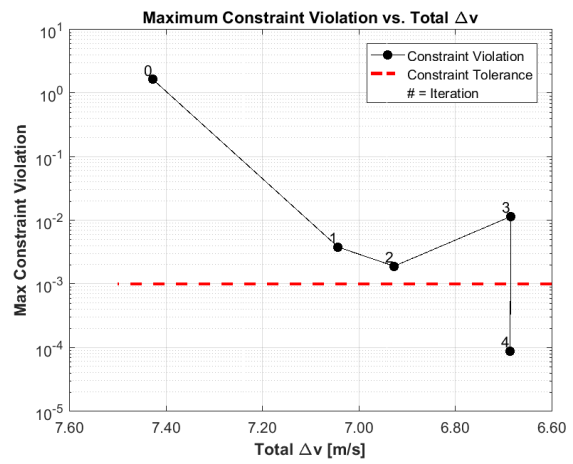
Figure 15: Total Δv vs. Iteration

Figure 16: Max Constraint Violation vs. Δv

trajectory propagation from t_0 to t_f. These gradients can then be utilized in any gradient-based solver to generate feasible or optimal burn solutions for ISS burn planning. Finally, the constraint gradient formulation can easily be extended to other functions of the state as needed.

ACKNOWLEDGMENTS

REFERENCES

[1] F. Sauceda, "Space Station Reference Coordinate Systems," Tech. Rep. SSP 30219, Revision F, October 26 2001.

[2] C. Ocampo and J. Munoz, "Variational Equations for a Generalized Spacecraft Trajectory Model," *Journal of Guidance, Control, and Dynamics*, Vol. 33, September-October 2010, pp. 1615–1618.

[3] T. J. Moesser, "Guidance and Navigation Linear Covariance Analysis for Lunar Powered Descent," 2010.